Materials Science for Energy Technologies 6 (2023) 399–408

Contents lists available at ScienceDirect

Materials Science for Energy Technologies

journal homepage: www.keaipublishing.com/en/journals/materials-science-for-energy-technologies

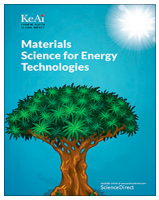

Ternary structured magnesium cobalt oxide/graphene/polycarbazole nanohybrids for high performance electrochemical supercapacitors

Akhil Babu [a], T.E. Somesh [a], C.D Ani Dechamma [a], A.B. Hemavathi [a,*], Raghava Reddy Kakarla [b], Raghavendra V. Kulkarni [c,d], Anjanapura V. Raghu [d,*]

[a] Department of Polymer Science and Technology, Sri Jayachamarajendra College of Engineering, JSS Science and Technology University, Mysore 570006, Karnataka, India
[b] School of Chemical and Biomolecular Engineering, The University of Sydney, Sydney, NSW 2006, Australia
[c] Department of Pharmaceutics, BLDEA's SSM College of Pharmacy and Research Centre, Vijayapur 586 103, Karnataka, India
[d] Faculty of Allied Health Sciences, BLDE (Deemed-to-be University), Vijayapura 586 103, India

ARTICLE INFO

Article history:
Received 26 January 2023
Revised 4 April 2023
Accepted 4 April 2023
Available online 7 April 2023

Keywords:
Polycarbazole
Conducting polymers
Metal oxide nanoparticles
Reduced graphene oxide
Ternary structured composites
Electrochemical property
Energy Density
Energy storage devices

ABSTRACT

In the present work, polycarbazole (PCz)/magnesium cobalt oxide ($MgCo_2O_4$)/reduced graphene oxide (RGO) based ternary nanocomposite was prepared through in-situ polymerization, and utilized it as an active electrodes for electrochemical energy storage supercapacitor applications. The electrochemical behaviour of PCz and its nanocomposites were investigated by measuring specific capacitance using cyclic voltammetry (CV), electrochemical impedance spectroscopy (EIS) and Galvanostatic charge–discharge (GCD) analysis. The PCz/$MgCo_2O_4$/RGO hybrids exhibited higher capacitance (548.54 F/g) than that of PCz (117.65 F/g) and PCz/$MgCo_2O_4$ (482.92 F/g) at the scan rate of 50 mV/s, as determined by CV method. The enhanced supercapacitance indicates high power and energy storage capabilities of the ternary metal oxide-graphene based polycarbazole nanocomposites. Electrochemical impedance spectroscopy confirmed low solution resistance of PCz/$MgCo_2O_4$/RGO. Thermogravimetric analysis affirmed the increased thermal stability of PCz/$MgCo_2O_4$/RGO composite compared to that of pure polycarbazole and PCz/$MgCo_2O_4$ nanocomposite. The scanning electron micrographs of nanocomposite confirmed the successful incorporation of nanofillers into the PCz matrix. On the basis of the research findings, PCz/$MgCo_2O_4$/RGO can be expected to be a promising electrode active material for high performance energy storage supercapacitors.

1. Introduction

Meeting the energy requirements of a rising population and technological advances is an important global challenge of the current century. Conventional sources of energy like natural gas, oil, and coal are diminishing at a faster rate, and their usage is also responsible for global warming. The development of wind, solar, biofuel, and other green energy sources is one way to address the existing energy crisis and environmental pollution disputes [1,2]. However, the utilization of clean energy sources is constrained by environmental factors, and the energy supply is intermittent. As science and technology develop rapidly over the years, there is an increasing need for reliable energy storage devices that can replace conventional batteries of low power density and dielectric capacitors of low energy density [1,3,4]. Supercapacitors or ultracapacitors are devices with superior capacitance, which overcomes the shortcomings of conventional batteries and dielectric capacitors by providing high energy storage density, high power density, and a number of other advantages including rapid charge–discharge capability, high power capacity and operation at a wide range of temperatures [5–7].

There are three different types of supercapacitors including pseudocapacitors, electrostatic double layer capacitors (EDLC) and hybrid capacitors [8–11]. In EDLC devices, the energy storage takes place at the electrolyte–electrode interface without charge transfer taking across the electrodes, and no redox reaction is involved. This mechanism is generally observed in carbon-based electrode active materials such as graphene, CNTs, and activated carbon [5,12]. Charge storage in a pseudocapacitor is the result of charge transfer between the electrode and electrolyte, which is achieved by a redox reaction occurring at the electrode surface [1,13]. The composite materials are used in hybrid supercapacitors,

* Corresponding authors.
E-mail addresses: hemavathi@sjce.ac.in (A.B. Hemavathi), gsraghu2003@yahoo.co.in (A.V. Raghu).

https://doi.org/10.1016/j.mset.2023.04.002
2589-2991/

which displays a combination of pseudocapacitor and EDLC mechanism. The composite materials are used in hybrid supercapacitors, which combine the pseudocapacitor and EDLC mechanisms. The composite materials are made up of carbon-based materials like graphene combined with metal oxides, conducting polymers, or both [14,15].

Carbon-based nanostructured materials such as CNTs, reduced graphene oxide, graphene and activated carbon are utilized as electrode active materials for EDLC owing to its good electrical properties, high specific surface area and nanoporosity [3,16,17]. Graphene and its derivatives such as graphene oxide (GO) and RGO have a high surface area and high conductivity owing to the presence of π-electrons. Also, RGOs have inherent functional groups exhibiting better supercapactive behaviour resulting in a higher power and energy density [18]. Conducting polymers such as polycarbazole, polypyrrole, polyaniline, polythiophene, and transition metal oxides such as TiO_2, ZnO, CuO, MnO_2, Fe_3O_4, and Co_3O_4 are employed as electrode active materials for pseudocapacitors [4,19,20].

Carbon-based materials used in EDLC provide high power density but low energy density, which lowers the overall performance of the supercapacitor [3,21,22]. Polycarbazole is a cost-effective polymer that is easy to process compared to other conducting polymers and also exhibits good electrical, thermal, and charge carrier properties in amalgamation with other carbon-based materials. It can be used in various applications such as light emitting diodes, biosensors, solar cells, and supercapacitors [23–26]. Although good conductivity and high capacitance can be obtained with the modification of conducting polymers, limited stability leads to degradation problems [27,28]. The addition of inorganic metal oxides improves the overall stability in such cases. Ternary metal oxides having two metal ions and the synergistic effect of elements possess higher electrical conductivity than binary metal oxides [29]. Spinel cobaltates (XCo_2O_4, where X = Ca, Mg, Ni) are gaining massive research interest owing to its low price, non-toxic nature, higher stability and enhanced electrochemical properties [30–32]. Despite their high specific capacitance, low cost and easy availability, metal oxides exhibit higher resistance and to overcome this drawback, the metal oxides are generally mixed/blended with carbon-based materials. A composite material comprising of metal oxide nanoparticles/conducting polymer/carbon-based materials can be a better combination to use as an electrode active material for electrochemical supercapacitor applications. These nanocomposites exhibit good synergistic effect, and improved conductivity as well can alter the storage properties of the electrode active material [33,34].

There are wide varieties of electrode active materials and electrolytes available. Hence, selecting the optimal electrode material is important in supercapacitor operation, and the overall performance of supercapacitor can be fine-tuned by changing the properties of electrode active material. To best of our knowledge, no reports are available on ternary hybrid electrode materials consisting of cobaltate, graphene and polycarbazole, leaving plenty of opportunity to investigate these materials for future practical applications. This study investigates PCz/$MgCo_2O_4$/RGO ternary nanocomposites as a potential active electrode material for electrochemical supercapacitor applications. Further, the synthesized nanocomposites were characterized using techniques such as XRD, FTIR, Raman spectroscopy, TGA, CV, GCD, and EIS analysis. Development of ternary metal oxide dispersed graphene-based polycarbazole hybrid nanocomposites based electrode material gives a good opportunity for practical applications of supercapacitors in hybrid electric vehicles, flywheels, wind turbines, kinetic energy recovery systems (KERS), and so on.

2. Materials and methods

2.1. Materials

Carbazole, magnesium nitrate tetrahydrate [$Mg(NO_3)_2{\cdot}4H_2O$], cobalt nitrate hexahydrate [$Co(NO_3)_2{\cdot}6H_2O$] (oxidants), and glycine [$C_2H_5NO_2$] (fuel), graphite flakes, sulphuric acid, tetrahydrofuran, chloroform were purchased from SD Fine Chemicals, Mumbai, India. Potassium permanganate, hydrogen peroxide, hydrochloric acid, ammonium dihydrogen phosphate, and methanol were procured from Nice Chemicals, Kochi, India. Double distilled water was used during the entire course of the experiment.

2.2. Methods

2.2.1. Synthesis of $MgCo_2O_4$ nanoparticles

The $MgCo_2O_4$ nanoparticle was synthesized by the solution combustion method [35]. The Mg $(NO_3)_2{\cdot}4H_2O$, and $Co(NO_3)_2{\cdot}6H_2O$ (oxidants) and glycine ($C_2H_5NO_2$) were taken in stoichiometric proportions. Oxidants and glycine were dissolved separately in double distilled water and stirred continuously for 30 min. The molar ratio of the oxidant to fuel used was 1:1. The individual solutions were mixed to obtain a combustion mixture with continuous stirring for 30 min. Further, the *p*H was adjusted in the range 8.5–9 by the addition of KOH solution. Then, the combustion mixture was subjected to vigorous stirring for 2 h at 90 °C until a dark gel was obtained. The gel is then heated until dry powder is formed. Finally, the dark grey powder was calcined at 650–800 °C for 4 h, and nanoparticles were obtained. Calcination was carried out to remove the impurities/unwanted reagents as well as to make the nanoparticles more stable.

2.2.2. Synthesis of RGO and $MgCo_2O_4$ decorated RGO

Graphene oxide (GO) was synthesized through the improved Hummers method [36]. Further (500 mg) of GO obtained was mixed with (60 mL) of distilled water and was ultra-sonicated for 20 min. 5 g of ammonium hydroxide was dissolved in 30 mL of distilled water, and was added to the GO solution, and sonicated for 20 min. Then, the solution was taken into a Teflon tube and kept in an oven at 170 °C for 12 h. Then, it was cooled to room temperature, centrifuged, washed, and dried to obtain the RGO in powder form. The magnesium cobalt oxide nanoparticles were decorated on GO by the solvothermal method [37]. The obtained $MgCo_2O_4$/GO was further reduced to $MgCo_2O_4$/RGO by hydrothermal method.

2.2.3. Synthesis of polycarbazole

The oxidative polymerization route was followed for the synthesis of polycarbazole [38]. About (1.67 g) of carbazole was dissolved in (50 mL) of chloroform. About 3.8 g of *p*TSA (dopant) dissolved separately in chloroform was added to above precursor solution and continuously stirred for 30 min. About 3.6 g of Benzoyl peroxide (initiator) dissolved in chloroform was added slowly to the above solution, which was then stirred for 4 hr. The color of the solution gradually changes to dark green, indicating the formation of PCz. The obtained dispersion was added to an excess of methanol to complete the polymerization reaction. The synthesized green precipitate was washed with ethanol and vacuum dried at 50 °C until it reached a constant weight.

2.2.4. Synthesis of PCz/$MgCo_2O_4$ and PCz/$MgCo_2O_4$ /RGO nanocomposites

The $MgCo_2O_4$ and $MgCo_2O_4$ decorated reduced graphene oxide incorporated polycarbazole nanocomposites were prepared by in-situ polymerization using benzoyl peroxide as the oxidizing agent

[39]. Carbazole monomer (1.67 g, 0.1 M), and *p*-Toluene sulfonic acid (3.8 g, 0.2 M), and (0.167 g) of $MgCo_2O_4$ nanoparticles were dispersed in (50 mL) of chloroform, and this mixture was constantly stirred for 1 h to obtain a homogenous dispersion. 50 mL of a chloroform solution containing BPO initiator (0.24 M, 3.6 g) was added drop by drop to the homogenous mixture. The reaction mixture was constantly stirred at ambient temperature for 4 hr, and the obtained dispersion was poured into an excess of methanol to complete polymerization. The resultant green precipitate was filtered, and washed several times with distilled water, followed by methanol. The powder sample was dried at 50 °C until it reached a constant weight. Similarly, $MgCo_2O_4$ decorated RGO incorporated polycarbazole nanocomposites were also synthesized. In the preparation of nanocomposites, initial trials were carried out with the incorporation of 25, and 10 wt% $MgCo_2O_4$, 25 and 10 wt% of $MgCo_2O_4$ decorated RGO. The preliminary results showed that 10 wt% is better with respect to dispersion and electrical properties, so in further studies, the same concentration is used.

2.2.5. Characterization

The structure of pristine $MgCo_2O_4$ and nanocomposites were ascertained by X-Ray diffraction pattern obtained from Proto AXRD table top diffractometer (Proto, Canada) in the 2θ range of 10-70° at the scan rate of 0.04° per second. FTIR spectra of pristine $MgCo_2O_4$ and nanocomposites were recorded in attenuated total reflectance mode to analyze the physical interactions between the components in the range of 4000 to 400 cm^{-1}. Raman analysis of the neat PCz and the nanocomposites were recorded (XPlora Plus, Japan) using 532 nm laser in the order of 0 to 3000 cm^{-1}. Electrochemical studies such as cyclic voltammetry, GCD, and electrochemical impedance spectroscopy (EIS) measurements were conducted in 1 M H_2SO_4 solution at various scan rates (50–1000 mV/s) in the potential range of −0.7 to 1.5 V using electrochemical analyzer (CHI608E, CH Instruments). The thermal stability of neat polycarbazole and nanocomposites were assessed using a thermogravimetric analyzer (Q50, TA Instruments, USA) in the temperature range of 25–800 °C at the heating rate of 20 °C/min under a nitrogen atmosphere. The morphology of the prepared nanocomposites was studied using a scanning electron microscope (JEOL, JSM-IT300, USA).

3. Results and discussion

3.1. Structural characterization

3.1.1. XRD analysis

The microstructural features of pristine $MgCo_2O_4$, neat PCz, and synthesized nanocomposites were studied using X-Ray diffraction. The resultant XRD profiles are shown in Fig. 1. Neat PCz shows a semicrystalline diffraction peak at 2θ value of 19.9° which originates from the ordering of N-H and O-H groups and the presence of hydrogen bonds in PCz [38]. There are also minor peaks at 2θ value of 31.3° and 42° which corresponds to small islets of crystalline portion dispersed in the amorphous region of PCz.

The prominent peaks of $MgCo_2O_4$ nanoparticles were observed at 36.95°, 42.85°, and 62.02°. The sharp and intense peaks of $MgCo_2O_4$ nanoparticles indicate the high crystalline nature of $MgCo_2O_4$ nanoparticles. The XRD pattern of nanocomposites indicates the modified structure of PCz in the presence of $MgCo_2O_4$ and $MgCo_2O_4$/RGO. The peaks of $MgCo_2O_4$ and $MgCo_2O_4$/RGO are also present in the nanocomposites. It is also observed that the semicrystalline peak intensity is reduced, and a broader peak is obtained in the nanocomposites, which could be due to intercalation between the nanoparticles and PCz chain and may also be due to the coating of $MgCo_2O_4$ by polycarbazole.

3.1.2. FTIR analysis

The FTIR studies give information about the effect and interactions between various constituents in polymer nanocomposites. Fig. 2 shows FTIR spectra of polycarbazole and its nanocomposites in a range of 4000–500 cm^{-1} wave number. The characteristic bands of neat PCz and its nanocomposites are detailed in Table 1. The observed peaks at 3405, 3045, 1725, 1607, 1396, 1060, and 806 cm^{-1} are assigned to signature bands of polycarbazole. The observed strong bands from 3100 cm^{-1} to 3410 cm^{-1} correspond to the vibrational stretching of N-H group [40]. The aromatic

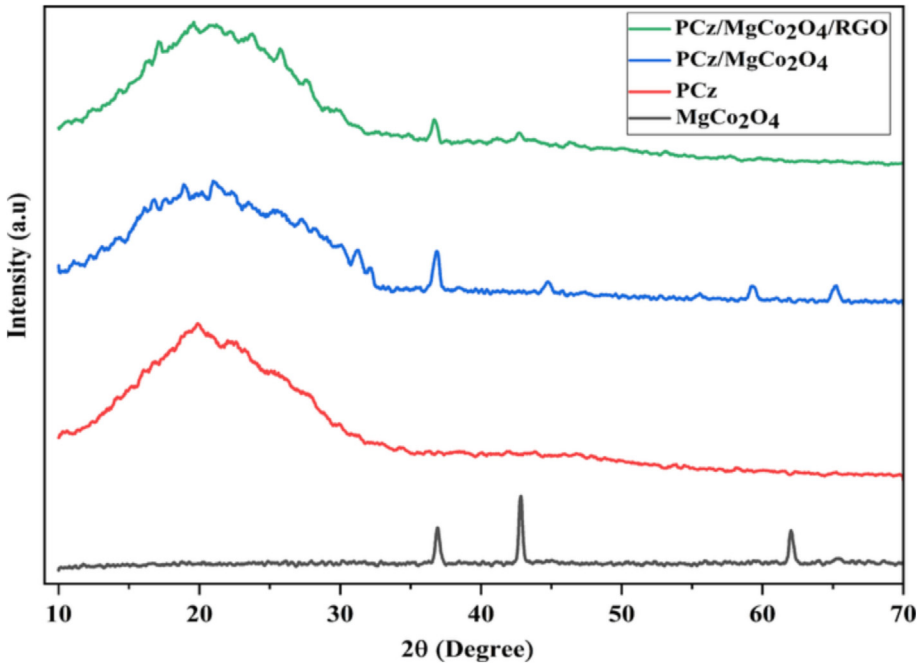

Fig. 1. The XRD spectra of pristine $MgCo_2O_4$, neat PCz and nanocomposites.

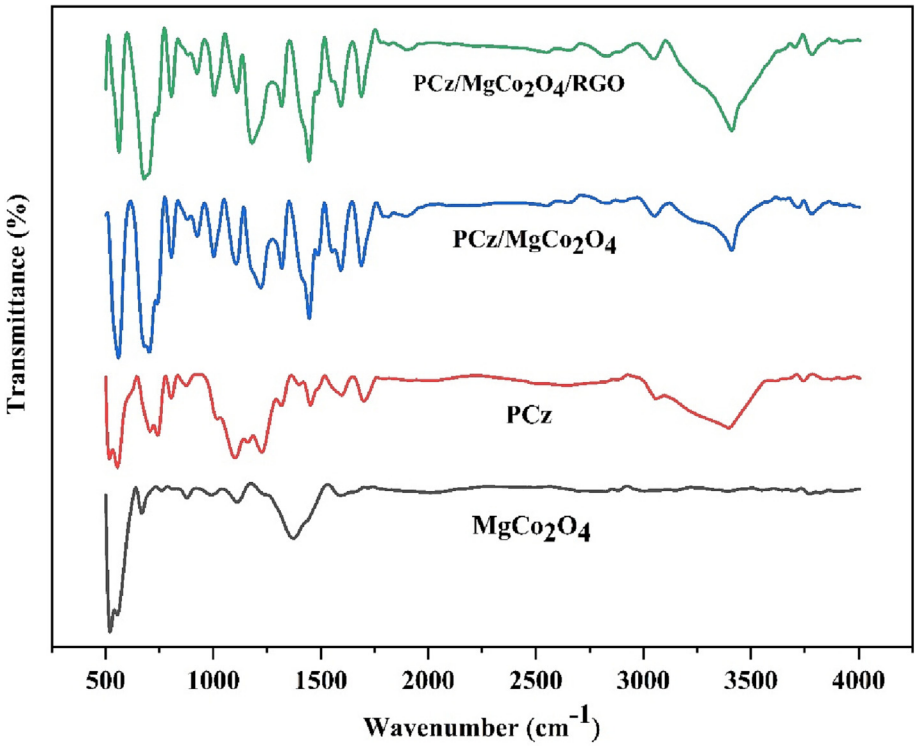

Fig. 2. The FTIR spectra of $MgCo_2O_4$, PCz, PCz/$MgCo_2O_4$, PCz/$MgCo_2O_4$/RGO.

Table 1
The FTIR peak analysis of neat PCz, PCz/$MgCo_2O_4$, and PCz/$MgCo_2O_4$/RGO.

Characteristic peak	Peak position (cm^{-1})		
	PCz	PCz/$MgCo_2O_4$	PCz/$MgCo_2O_4$/RGO
N-H Stretching	3401	3413	3409
Aromatic C—H Stretching	3054	3046	3046
C=O Stretching	1700	1689	1689
	1604	1596	1593
Aromatic C—N Stretching	1450	1446	1446
S=O group	1096	1104	1100
C—H Deformation	810	806	806
O—Co—O vibrations	–	555	563
		682	674

C—H stretching occurs at 3045 cm^{-1} while the C=O stretching due to over oxidation was observed at 1725 $cm^{-1,}$ and aromatic stretching of C=C double bond occurs at 1607 cm^{-1}. The oxidative polymerization of monomers into a continuous chain and the aromatic ring structure occurs at 1450 cm^{-1} and C—N stretching occurs at 1396 cm^{-1} [41]. The doping of polycarbazole is evident from 1060 cm^{-1} peak, which corresponds to S=O vibrations of *p*TSA (doping agent) [38]. From the spectra, it can be observed that the structure of PCz is affected by the addition of $MgCo_2O_4$ nanoparticle and $MgCo_2O_4$ decorated RGO. For pristine $MgCo_2O_4$ nanoparticles, the peak at 1600 cm^{-1} and 3401 cm^{-1} corresponds to the adsorption of water, and the peaks at 668 cm^{-1} and 555 cm^{-1} correspond to O-Co-O vibrations [42]. For the PCz/$MgCo_2O_4$ nanocomposites, the peak corresponding to N-H stretching was shifted to a higher wave number of 3413 cm^{-1}. The peaks at 806 cm^{-1} are attributed to the C—H deformation in trisubstituted benzene rings. For PCz/$MgCo_2O_4$/RGO nanocomposites, a broad peak was observed between 3100 and 3400 cm^{-1} due to the adsorbed water on the graphene oxide surface, and the peak at 3409 cm^{-1} corresponds to N-H stretching. For RGO, the spectrum corresponding to C=C bond was observed at 1546 cm^{-1}. The peak at 1446 cm^{-1} corresponds to the C—N stretching of aromatic C—N bonds [40,41].

All the nanocomposites exhibit two peaks at around 558 and 682 cm^{-1} which confirms the presence of the metal oxide nanoparticles. The FTIR spectra of neat PCz and nanocomposites show a shift in peak position as well as a change in intensity. This reveals that PCz/$MgCo_2O_4$ and PCz/$MgCo_2O_4$/RGO are not a simple mixture of PCz matrix, $MgCo_2O_4$ nanofiller, and $MgCo_2O_4$ decorated RGO but a composite of PCz matrix with dispersed nanofillers.

3.1.3. Raman spectroscopic analysis

The interaction between polymer chains and $MgCo_2O_4$ nanoparticles as well as with $MgCo_2O_4$ decorated RGO were studied using Raman spectroscopy. The Raman spectra of PCz, PCz/$MgCo_2O_4$, and PCz/$MgCo_2O_4$/RGO are shown in Fig. 3. The detailed peak analysis of the neat polycarbazole as well as the nanocomposites are shown in Table 2.

The Raman spectra of nanocomposites exhibited two typical peaks corresponding to D and G bands which appeared at 1336 cm^{-1} and 1554 cm^{-1}. The D band corresponds to stretching vibrations of C—C or defects in the hexagonal lattice, whereas G band corresponds to in plane vibrations of sp^2 bonded carbon atom [43]. The peaks at 570, 671 and 845 cm^{-1} correspond to metal–oxygen bond of $MgCo_2O_4$ nanoparticles. For polycarbazole, the peak observed at 1336, and 1563 cm^{-1} are attributed to the ring stretching and C=C backbone. The peak at 2776 cm^{-1} corresponds to 2D band, 935 cm^{-1} to the bipolaron ring deformation, and 1060 cm^{-1} corresponds to C—H in-plane vibrations. After the incorporation of $MgCo_2O_4$ into RGO, there is a shift in the D and G bands, which appeared at 1355 and 1569 cm^{-1} in the nanocomposites. The Raman spectra of nanocomposites show a band of polycarbazole and hence confirmed the presence of PCz in nanocomposites. The I_D/I_G ratio, which provides information about the extent of disordered carbon for the neat PCz was 0.89, whereas that obtained for PCz/$MgCo_2O_4$ and PCz/$MgCo_2O_4$/RGO was 0.94 and 0.98, respectively [44]. It was also observed that the intensity

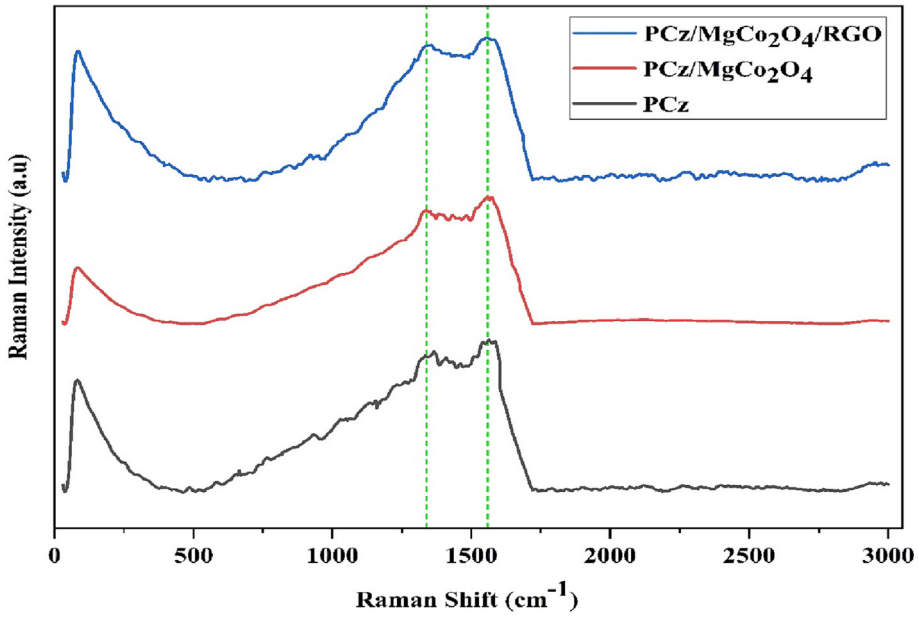

Fig. 3. Raman spectra of PCz, PCz/$MgCo_2O_4$, PCz/$MgCo_2O_4$/RGO.

Table 2
Raman spectra analysis of neat PCz, PCz/$MgCo_2O_4$, and PCz/$MgCo_2O_4$/RGO.

Characteristic band and I_D/I_G ratio	Raman Shift (cm^{-1})		
	PCz	PCz/$MgCo_2O_4$	PCz/$MgCo_2O_4$/RGO
D-Band	1336	1359	1355
G-Band	1563	1569	1569
I_D/I_G Ratio	0.89	0.94	0.98

of D band is enhanced for nanocomposites which indicates better interaction between $MgCo_2O_4$ nanoparticles, RGO, and polycarbazole. The bands in the range 640–560 cm^{-1} show an increase in intensity and shift to a lower wave number, which indicates that $MgCo_2O_4$ and $MgCo_2O_4$/RGO addition has an impact on PCz matrix.

3.2. SEM analysis

The morphology of synthesized samples was investigated using a scanning electron microscope (SEM). The SEM micrographs of PCz, PCz/$MgCo_2O_4$ and PCz/$MgCo_2O_4$/RGO were shown in Fig. 4**(a-c)**. The SEM images of nanocomposite indicated the successful distribution of nanofillers into the PCz matrix. The incorporation of $MgCo_2O_4$ and $MgCo_2O_4$/RGO nanofillers into PCz matrix is expected to improve the capacitive behaviour of synthesized nanocomposite. From Fig. 4**(a)**, it can be observed that a flocculent or nodular morphology was displayed in the case of neat PCz.

Upon incorporation of $MgCo_2O_4$ nanofillers into the polycarbazole matrix, it was observed that the $MgCo_2O_4$ nanoparticles were adsorbed on the surface of polycarbazole. From Fig. 4**(c)**, it can be observed that the RGO has crumbled sheet-like morphology and upon which $MgCo_2O_4$ nanofillers were deposited. The enhanced surface area of RGO facilitates the even distribution of $MgCo_2O_4$ NPs. The morphological effect is also reflected in the capacitance value of the nanocomposites, wherein the maximum capacitance is obtained for PCz/$MgCo_2O_4$/RGO.

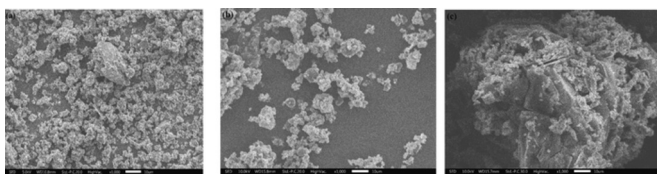

Fig. 4. SEM micrographs of (a) neat PCz, (b) PCz/$MgCo_2O_4$, and (c) PCz/$MgCo_2O_4$/RGO.

3.3. TGA analysis

Thermogravimetric analysis was carried out to probe the thermal stability of neat PCz and its nanocomposites. TGA thermogram of neat PCz, PCz/$MgCo_2O_4$, and PCz/$MgCo_2O_4$/RGO has been shown in Fig. 5. From the thermogram, it is evident that there is an initial minor weight loss in the temperature range of 27–100 °C due to loss of moisture and absorbed water [45]. The second stage of weight loss occurred in the range of 100–230 °C, which indorses to the degradation of low molecular weight PCz chains. In the third stage, a massive mass loss was observed, which is due to the breakdown of longer PCz chain [46].

After the incorporation of $MgCo_2O_4$ and $MgCo_2O_4$ decorated RGO into the PCz matrix, the thermal property of PCz was enhanced. The estimated total mass loss at 900 °C in the neat polycarbazole, PCz/$MgCo_2O_4$, and PCz/$MgCo_2O_4$/RGO nanocomposites were 76.8%, 64.3%, and 38.8%, respectively.

3.4. Electrochemical tests

An electrochemical analyzer with a standard 3-electrode system was used to test the electrochemical properties of the polymer and nanocomposites. The caramel mercury electrode, glassy carbon electrode, and platinum wire were utilized as the reference electrode, working electrode, and counter electrode, respectively. For the preparation of the working electrode, a known amount of electrode active material (5 mg) was dispersed in 1 mL of ethanol, and further, the mixture was cast on a glassy carbon electrode, then it was dried at room temperature for 2 hr. The samples were analyzed by cyclic voltammetry (CV), galvanostatic charge–discharge (GCD), and electrochemical impedance spectroscopy.

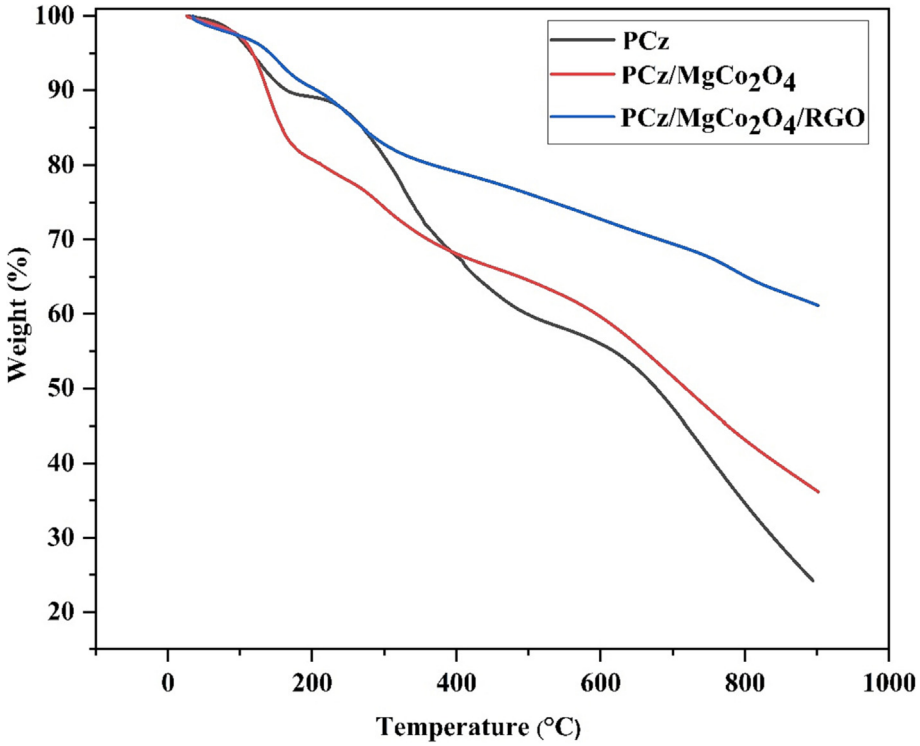

Fig. 5. TGA thermogram of PCz, PCz/$MgCo_2O_4$ and PCz/$MgCo_2O_4$/RGO.

3.4.1. CV analysis

The CV measurement was carried out using a standard 3-electrode system at different scan rates of 50, 100, 200, 500, and 1000 mV/s in the potential range of −0.7 to 1.5 V. The specific capacitance (C_{sp}) was calculated from equation (1).

$$Csp = \left(\int IdV\right)/(m\ v\ \Delta V) \quad (1)$$

where, ($\int$I dV) is the integral area of CV curve, 'm' is the total mass of electrode active material (g), 'ν' is the scan rate (mV/s) and 'ΔV' is the range of potential window. The CV plots of neat PCz, PCz/$MgCo_2O_4$, and PCz/$MgCo_2O_4$/RGO at 100 mV/s are shown in Fig. 6 **(a)**. PCz/$MgCo_2O_4$/RGO exhibits a rectangular profile, which indicates ideal capacitive behavior and low contact resistance. RGO and $MgCo_2O_4$ nanoparticles are responsible for both EDLC and pseudocapacitive behavior. The redox peak is also clearly visible [43]. The specific capacitance (C_{sp}) at a scan rate of 100 mV/s for neat PCz, PCz/$MgCo_2O_4$, and PCz/$MgCo_2O_4$/RGO were 94.54, 389.82, and 455.23F/g, respectively. A higher capacitance was shown by PCz/$MgCo_2O_4$/RGO, which can be attributed to faradaic charge transfer due to the pseudo-capacitive behaviour of $MgCo_2O_4$. The addition of RGO increased the specific capacitance, which is ascribed to the electrochemical double layer capacitance.

It can be seen from Fig. 6**(b)** that the capacitance decreases with an increase in the scan rate due to faster diffusion of the ions at the electrodes. The ions H^+, HSO_4^-, and SO_4^{2-} present in the electrolyte do not get sufficient time to accumulate on the electrode surface, resulting in lower C_{sp} values at higher scan rates [47]. The synergistic effect of $MgCo_2O_4$ and RGO with polycarbazole resulted in a higher electrochemical capacitive performance of the nanocomposites. The energy density (E) and power density (P) of pure polycarbazole and nanocomposites can be calculated from the CV data using equations (2) and (3), respectively.

$$E = 0.5\ Csp\ \Delta V^2 \quad (2)$$

$$P = E * 3600/\Delta t \quad (3)$$

where 'C_{sp}' is the specific capacitance, 'ΔV' is the potential window and 'Δt' is the discharge time. From the Ragone plot, Fig. 6**(c)**, it can be observed that PCz/$MgCo_2O_4$/RGO exhibits a higher power density of 102.39 W/kg and an energy density of 0.347 Wh/kg. The maximum power density of PCz and PCz/$MgCo_2O_4$ is 20.01 and 100.1 W/kg, respectively. The maximum energy density for PCz and PCz/$MgCo_2O_4$ are 0.7206 and 0.324 Wh/kg, respectively.

3.4.2. GCD analysis

The Galvanostatic charge–discharge analysis has been carried out for neat PCz and its nanocomposites from 0.1 to 10 mA, and the capacitance is calculated using the equation (4).

$$C = (I\ \Delta t)/(\Delta v\ m) \quad (4)$$

where 'I' is the applied current, 'Δt' is the discharge time from the highest value of potential to the lowest potential, 'ΔV' is the potential window, and 'm' is the total mass of sample. The capacitance of PCz was enhanced upon addition of $MgCo_2O_4$ decorated RGO, which can be attributed to the conductive nature of RGO and $MgCo_2O_4$, which resulted in better ion diffusion into the electrode active material as well as the synergistic effect among three components of PCz/$MgCo_2O_4$/RGO composite. All GCD curves are of similar shape, as shown in Fig. 7, which indicates that electrode material has an ideal capacitive behaviour. The shape obtained is deviated from perfectly triangular, which is attributed to faradaic and non-faradaic charge behaviour of PCz and $MgCo_2O_4$. Among the synthesized electrode material, the discharge time of PCz/$MgCo_2O_4$/RGO is maximum, indicating its best electrochemical performance. The specific capacitance at 1 mA for PCz, PCz/$MgCo_2O_4$, and PCz/$MgCo_2O_4$/RGO are 92.72, 445.66, and 516.53 F/g, respectively. With an increase in the applied current, there was a gradual decrease in capacitance, consistent with the inverse relationship between current and capacitance.

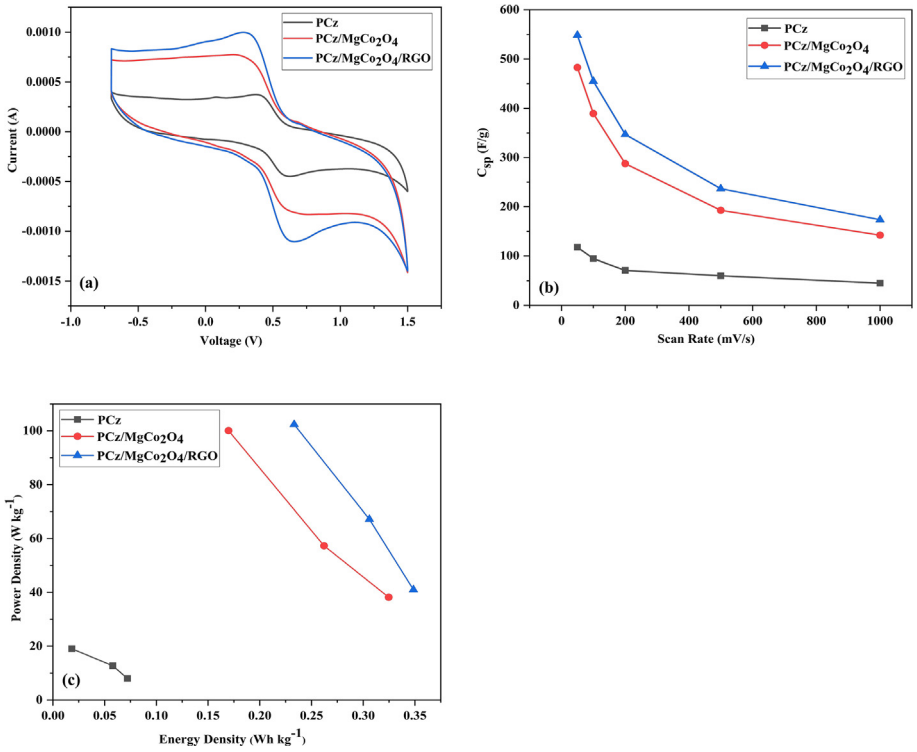

Fig. 6. (a) The CV curves at 100 mV/s for neat PCz, PCz/$MgCo_2O_4$, and PCz/$MgCo_2O_4$/RGO, (b) Variation of specific capacitance with the scan rate, (c) Ragone Plot for neat PCz, PCz/$MgCo_2O_4$, and PCz/$MgCo_2O_4$/RGO.

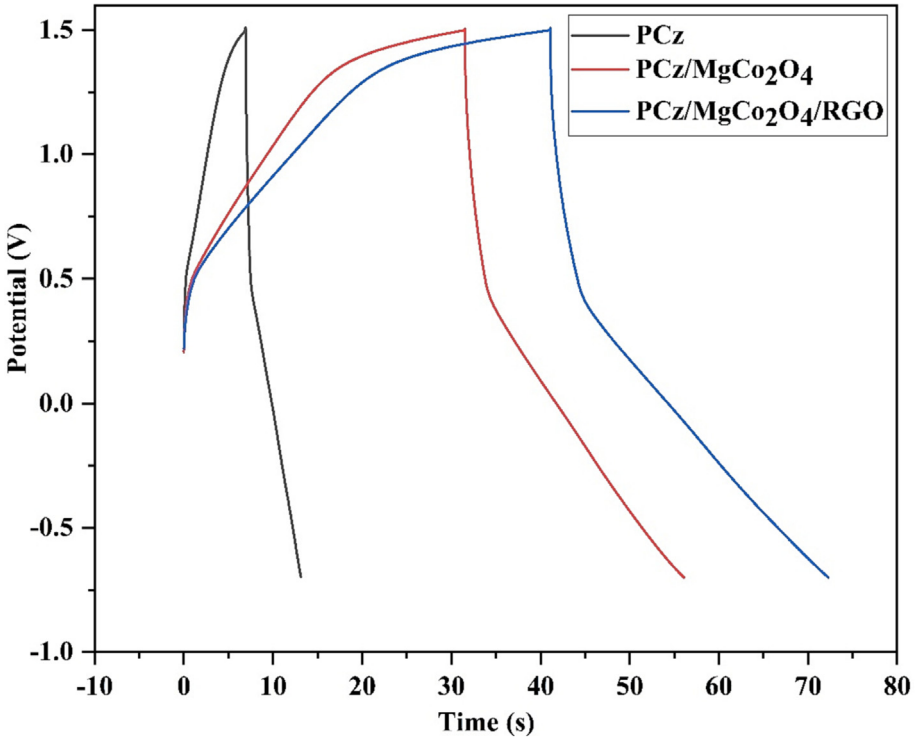

Fig. 7. Potential Vs time plot of GCD analysis at 1 mA.

3.4.3. EIS analysis

Electrochemical impedance spectroscopy provides information on electrode surface impedance changes and charge transfer phenomena that occur at the electrode–electrolyte interface. The analysis was carried out in 1 M H_2SO_4 using a standard 3-electrode system in the frequency range of 0.1 to 10^5 Hz. The Nyquist plot, a relation between imaginary impedance (Z") and real impedance (Z′) of neat PCz and nanocomposites are shown in Fig. 8. From the Nyquist plot, it can be observed that there is a straight line with an angle of 45° in the lower frequency region, which stipulates the good capacitive nature of the polymer as well as the nanocomposites and semi-circular regions at a higher frequency, which

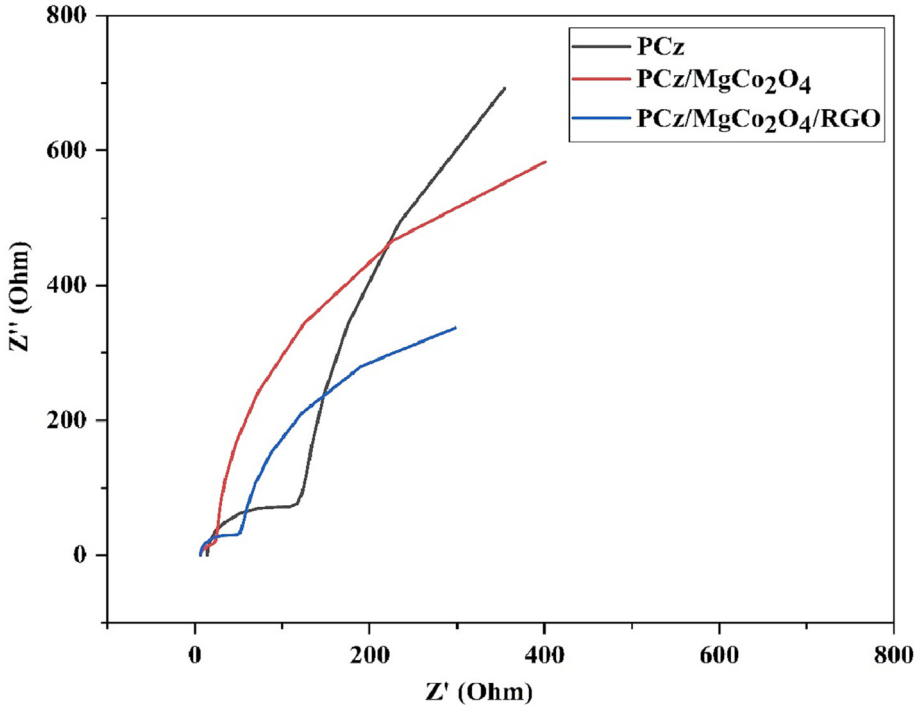

Fig. 8. The Nyquist plot of neat PCz, PCz/$MgCo_2O_4$, and PCz/$MgCo_2O_4$/RGO.

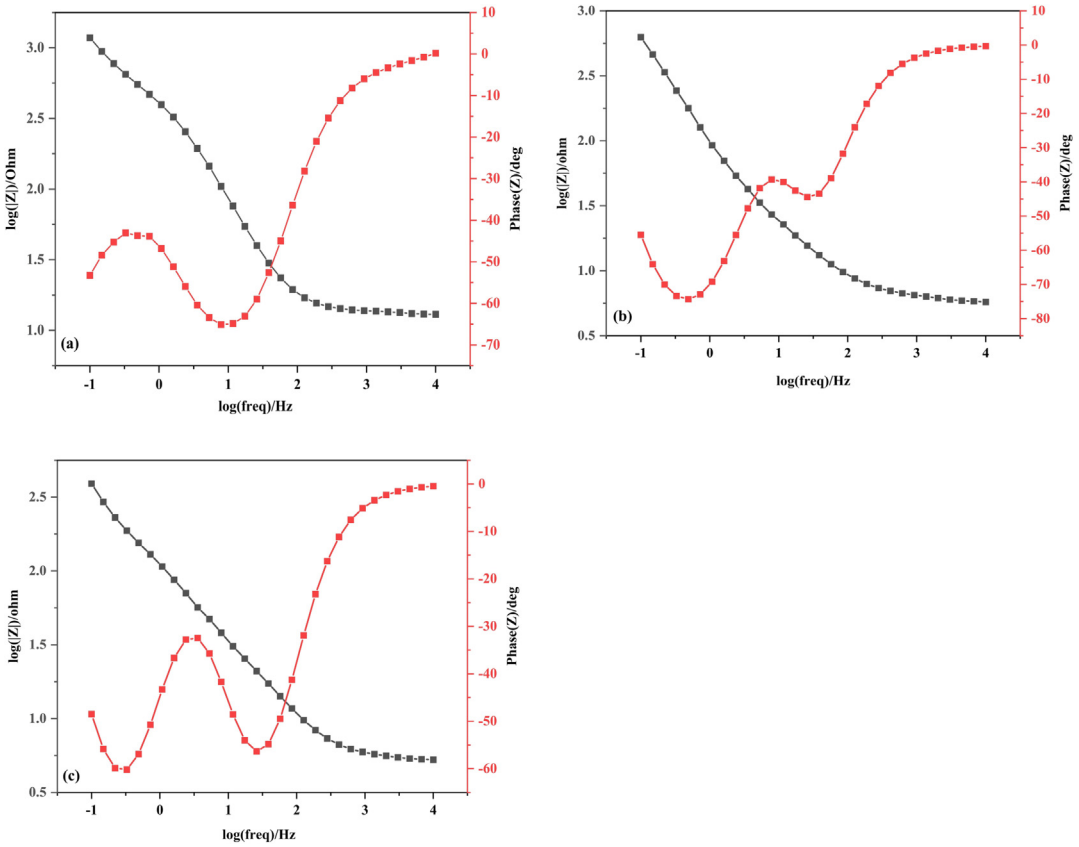

Fig. 9. The Bode magnitude and phase plot of (a) PCz, (b) PCz/$MgCo_2O_4$, and (c) PCz/$MgCo_2O_4$/RGO.

attributes to low charge transfer resistance [48]. It can be seen that PCz/$MgCo_2O_4$/RGO had a low solution resistance of 5.96 Ω, while PCz/$MgCo_2O_4$ and PCz had a higher solution resistance of 6.44 and 13.94 Ω, respectively.

The solution resistance was deducted from the x-axis intercept of Nyquist plot in the region of lower frequency. A lower solution resistance for PCz/$MgCo_2O_4$/RGO was achieved with the introduction of RGO, a graphene derivative that imparts more active sites

to electrolyte ions on the electrode and electrolyte surface [49]. The presence of RGO also helps to stabilize the metal oxides [50]. It can be inferred that PCz/$MgCo_2O_4$/RGO is a more suitable electrode active material compared to the other materials under study.

Additional information about the performance of electrode active materials can be derived from Bode magnitude and phase plots. The Bode plots of neat polycarbazole, PCz/$MgCo_2O_4$, and PCz/$MgCo_2O_4$/RGO are depicted in Fig. 9**(a), (b) and (c)**, respectively. According to the Bode phase and magnitude plots, the phase angles of all the electrodes are in the order of −45°, indicating the pure capacitive nature of electrodes. Also, from the plot, it is observed that amplitude set against frequency exhibits three different slopes at different regions. The electrode material possessing the least slope in the high-frequency region can be considered as a material with better electrochemical properties [51–55]. The PCz/$MgCo_2O_4$/RGO exhibit the least slope (-0.12) compared to PCz (-0.05) and PCz/$MgCo_2O_4$ (-0.10) which specifies better electrochemical properties of PCz/$MgCo_2O_4$/RGO.

4. Conclusions

PCz, PCz/$MgCo_2O_4$ and PCz/$MgCo_2O_4$/RGO were synthesized as electrode active materials for electrochemical energy storage supercapacitor applications. The XRD and FTIR analysis confirms the successful incorporation of $MgCo_2O_4$ and $MgCo_2O_4$ decorated RGO into the PCz matrix. XRD pattern shows an increase in the crystallinity of the nanocomposites compared to pure polycarbazole. The FTIR analysis confirms the functional bonds, which are unaffected by the incorporation of fillers into the PCz matrix. TGA analysis confirms that the thermal stability of PCz/$MgCo_2O_4$/RGO ternary composite is higher than that of neat polycarbazole and PCz/$MgCo_2O_4$ nanocomposite. It could also be observed that PCz/$MgCo_2O_4$/RGO nanocomposites exhibited higher capacitance compared to pristine polycarbazole and PCz/$MgCo_2O_4$ at the scan rate of 50 mV/s. Electrochemical impedance spectroscopy confirms low solution resistance of PCz/$MgCo_2O_4$/RGO. These findings indicate that PCz/$MgCo_2O_4$/RGO ternary hybrids are potentially useful electrode active materials for electrochemical energy storage systems.

Funding

No funding was received for conducting this study.

CRediT authorship contribution statement

Akhil Babu: Conceptualization, Methodology, Writing – original draft. **T.E. Somesh:** Investigation. **C.D Ani Dechamma:** Software. **A.B. Hemavathi:** Formal analysis, Visualization, Writing – review & editing. **Raghava Reddy Kakarla:** Methodology, Writing – review & editing. **Raghavendra V. Kulkarni:** Formal analysis. **Anjanapura V. Raghu:** Supervision, Writing – review & editing.

Declaration of Competing Interest

The authors declare that they have no known competing financial interests or personal relationships that could have appeared to influence the work reported in this paper.

Acknowledgments

A.V.R is thankful to KSCST, Government of Karnataka for awarding Sir C. V. Raman award for young scientist award in chemical sciences.

References

[1] C.V. Reddy, I.N. Reddy, K. Ravindranadh, B. Akkinepally, F. Alonso-Marroquin, K.R. Reddy, B. Cheolho, J. Shim, Sol. Energy Mater. Sol. Cells 226 (2021) 111056.
[2] U. Bharagav, N.R. Reddy, V.N.K. Rao, P. Ravi, M. Sathish, D. Rangappa, K. Prathap, C.S. Chakra, M.V. Shankar, L. Appels, T.M. Aminabhavi, R.R. Kakarla, M. M. Kumari, Chemosphere 311 (2023) 137030.
[3] M. Cakici, R.R. Kakarla, F. Alonso-Marroquin, Chem. Eng. J. 309 (2017) 151–158.
[4] C.V. Reddy, K.R. Reddy, R.R. Zairov, B. Cheolho, J. Shim, T.M. Aminabhavi, J. Environ. Manage. 315 (2022) 115120.
[5] A. Mishra, N.P. Shetti, S. Basu, K. Raghava Reddy, T.M. Aminabhavi, ChemElectroChem 6 (23) (2019) 5771–5786.
[6] E.S. Greenhalgh, S. Nguyen, M. Valkova, N. Shirshova, M.S. Shaffer, A.R. Kucernak, Compos. Sci. Technol. (2023) 109968.
[7] K. Shireesha, T.R. Kumar, T. Rajani, C.S. Chakra, M.M. Kumari, V. Divya, K. Raghava Reddy, Crystals 11 (9) (2021) 1144.
[8] N.R. Reddy, A.S. Kumar, P.M. Reddy, R.R. Kakarla, S.W. Joo, T.M. Aminabhavi, J. Environ. Manage. 325 (2023) 116650.
[9] C. Lekakou, C.O. Moudam, F. Markoulidis, T. Andrews, J.F. Watts, G.T. Reed, J. Nanotechnol. 2011 (2011) 1–8.
[10] N.P. Shetti, S. Dias, K.R. Reddy, Mater. Sci. Semicond. Process. 104 (2019) 104684.
[11] K. R. Reddy, F. Alonso-Marroquin, *AIP Conference Proceedings* 2017, Vol. 1856, No. 1, 020003. AIP Publishing LLC.
[12] G. Wang, L. Zhang, J. Zhang, Chem. Soc. Rev. 41 (2012) 797–828.
[13] T. Purkait, G. Singh, D. Kumar, M. Singh, R.S. Dey, Sci. Rep. 8 (2018) 1–13.
[14] X. Chen, R. Pauli, L. Dai, Nat. Sci. Rev. 4 (2017) 453–489.
[15] M. Inagki, H. Konno, O. Tanaike, J. Power Sources 194 (2010) 7880–7903.
[16] S. Iqbal, H. Khatoon, A.H. Pandit, S. Ahmad, Mater. Sci. Energy Technol. 2 (3) (2019) 417–428.
[17] L.L. Zhang, X.S. Zhao, Chem. Soc. Rev. 38 (2009) 2520–2531.
[18] A. Manalu, K. Tarigan, S. Humaidi, M. Ginting, I.P. Manalu, Ikhwanuddin, Mater. Sci. Energy Technol. 5 (2022) 444–451.
[19] K.R. Reddy, K.P. Lee, A.I. Gopalan, A.M. Showkat, Polym. J. 38 (4) (2006) 349–354.
[20] L. Bach-Toledo, B.M. Hryniewicz, L.F. Marchesi, L.H. Dall'Antonia, M. Vidotti, F. Wolfart, Mater. Sci. Energy Technol. 3 (2020) 78–90.
[21] Y. Han, L. Dai, Macromol. Chem. Phys. 220 (2019) 1800355.
[22] Y. Wu, C. Cao, Sci. China Mater. 61 (2018) 1517–1526.
[23] T.Y. Chu, S. Alem, S.W. Tsang, S.C. Tse, S. Wakim, J. Lu, G. Dennler, D. Waller, R. Gaudiana, Y. Tao, Appl. Phys. Lett. 98 (2011) 115.
[24] F. Bekkar, F. Bettahar, I. Moreno, R. Meghabar, M. Hamadouche, E. Hernaez, J.L. Vilas-Vilela, L. Ruiz-Rubio, Polymers 12 (2020) 2227.
[25] B. Gupta, R. Gupta, Synth. Met. 160 (2010) 523–528.
[26] K.R. Reddy, K.P. Lee, A.G. Iyengar, J. Appl. Polym. Sci. 104 (6) (2007) 4127–4134.
[27] R. Holze, Y.P. Wu, Electrochim. Acta 122 (2014) 93–107.
[28] K.R. Reddy, K.P. Lee, A.I. Gopalan, A.W. Showkat, Polym. Adv. Technol. 18 (1) (2007) 38–43.
[29] I. Bilecka, I. Djerdj, M. Niederberger, Chem. Commun. 7 (2008) 886–888.
[30] A.R. Patel, G. Sereda, S. Banerjee, Curr. Pharm. Biotechnol. 22 (2021) 773–792.
[31] V. Jose, V. Jose, C.E. Freeda Christy, A.S. Nesaraj, Inorg. Nano-Met. Chem. 52 (12) (2022) 1449–1462.
[32] S.G. Krishnan, A. Arulraj, M. Khalid, M.V. Reddy, R. Jose, Renewable Sustainable Energy Rev. 141 (2021) 110798.
[33] A. Ehsani, A.A. Heidari, H. Mahdavi, M. Bigdeloo, M. Kalhor, Appl. Nanosci. 11 (2021) 2459–2467.
[34] M. Ates, S. Caliskan, E. Ozten, J. Solid State Electrochem. 22 (2018) 3261–3271.
[35] A. Varma, A.S. Mukasyan, A.S. Rogachev, K.V. Manukyan, Chem. Rev. 116 (2016) 14493–14586.
[36] J. Chen, B. Yao, C. Li, G. Shi, Carbon 64 (2013) 225–229.
[37] R. Atchudan, T.N. Edison, S. Perumal, D. Karthikeyan, Y.R. Lee, J. Photochem. Photobiol. B: Biol 162 (2016) 500–510.
[38] R. Boddula, P. Srinivasan, Int. Sch. Res. Notices 2014 (2014) 1–8.
[39] M. Das, S. Roy, Mater. Today: Proc. 18 (2019) 5438–5446.
[40] V. Raj, D. Madheswari, M.M. Ali, J. Appl. Polym. Sci. 116 (2010) 147–154.
[41] M. Ates, N. Uludag, Int. J. Polym. Mater. 64 (2015) 755–761.
[42] M. Hafeez, R. Shaheen, B. Akram, S. Haq, S. Mahsud, S. Ali, R.T. Khan, Mater. Res. Express 7 (2020) 025019.
[43] T.E. Somesh, T.D. Siddaramaiah, J. Solid State Chem. 309 (2022) 122824.
[44] M.Q. Al-Gunaid, A. Saeed, N.K. Subramani, B.S. Madhukar, J. Mater. Sci. Mater. Electron 28 (2017) 8074–8086.
[45] M. Das, S. Ghosh, S. Roy, New J. Chem. 42 (2018) 6918–6931.
[46] D.B. Kayan, V. Polat, Turk. J. Chem. 41 (2017) 233–242.
[47] X. Lu, H. Dou, C. Yuan, S. Yang, L. Hao, F. Zhang, L. Shen, L. Zhang, X. Zhang, J. Power Sources 197 (2012) 319–324.
[48] S. Sarker, A.J. Ahammad, H.W. Seo, D.M. Kim, Int. J. Photoenergy 2014 (2014) 1–17.
[49] T. Cetinkaya, R.A. Dryfe, J. Power Sources 408 (2018) 91–104.
[50] S.G. Krishnan, M. Harilal, A. Yar, B.L. Vijayan, J.O. Dennis, M.M. Yusoff, R. Jose, Electrochim. Acta 243 (2017) 119–128.
[51] R. Ramachandran, M. Saranya, A.N. Grace, F. Wang, RSC Adv. 7 (2017) 2249–2257.

[52] S.G. Krishnan, M.V. Reddy, M. Harilal, B. Vidyadharan, I.I. Misnon, M.H. Ab Rahim, J. Ismail, R. Jose, Electrochim. Acta 161 (2015) 312–321.
[53] D.K. Kumar, D. Suazo-Davila, D. García-Torres, C.R. Cabrera, C.V. Reddy, K.R. Reddy, Mater. Lett. 314 (2022) 131890.
[54] K. Kannan, D. Radhika, A.S. Nesaraj, K.K. Sadasivuni, K.R. Reddy, D. Kasai, A.V. Raghu, Mater. Sci. Energy Technol. 3 (2020) 853–861.
[55] R. Prabhu, B. Roopashree, T. Jeevananda, S. Rao, K.R. Reddy, A.V. Raghu, Mater. Sci. Energy Technol. 4 (2021) 92–99.